Supergranule Lifetime and Angular Momentum Transport

J. G. Beck

W. W. Hansen Experimental Physics Laboratory,
Stanford University, Stanford, CA 94305-4085

R. K. Ulrich

Department of Physics and Astronomy,
University of California, Los Angeles, CA 90095-1592

F. Hill

National Solar Observatory, NOAO, Tucson, AZ 85726

and

R. S. Bogart

W. W. Hansen Experimental Physics Laboratory,
Stanford University, Stanford, CA 94305-4085

ABSTRACT

Dopplergrams from the Michelson Doppler Imager (MDI) instrument on the SOHO mission show the existence of supergranules with lifetimes in excess of 5 days; with many supergranules having lifetimes over 2 days. Supergranules originate at points and grow larger in the early stage of evolution and either break up, contract back to a point, or fade at the end. Many new supergranules are formed at boundaries of older supergranules. We find a correlation between the north-south and east-west velocities which is consistent with an angular momentum transport mechanism which could sustain the sun's differential rotation.

Subject headings: Convection — Sun: atmospheric motions — Sun: photosphere — Sun: rotation

1. Introduction

Hart (1954, 1956) first detected supergranules, finding a photospheric velocity field with a size scale of 26,000 km, a lifetime of several hours and an amplitude of 170 $\mathrm{m\,s^{-1}}$. Leighton, Noyes and Simon (1962) subsequently, detected these features, finding cells with diameters of

30,000 km, rms velocities of 500 $\mathrm{m\,s^{-1}}$ and lifetimes of 10^4 to 10^5 seconds; they attributed it to convection. Simon and Leighton (1964) measured a mean lifetime of 20 hours and reported a strong spatial correspondence of supergranule cells boundaries with the magnetic network. Since the cells were irregularly shaped and had a large horizontal extent in comparison to the lifetime and vertical velocity, Simon and Leighton suggested that supergranulation appeared to be non-stationary convection. Since the detection of supergranulation, little other than their existence is undisputed. Controversy abounds regarding the convective nature, depth, horizontal size scale, and lifetime of supergranules.

If supergranules are convection cells they should have a temperature gradient. However, attempts to detect a temperature contrast (eg. Simon and Leighton, 1964; Beckers, 1968; Worden, 1975; and Foukal and Fowler, 1984) have produced inconclusive results. One of the best measurements was by Lin and Kuhn (1992) which established an upper limit of the temperature contrast of 3K. Additionally, Duvall *et al.* (1997) used time-distance helioseismology to examine the depths of supergranules and found that the thermal structure was not consistent with convection. Supergranules are not the only velocity features suspected of being convective without direct evidence of convection: the recently detected giant cells (Ulrich 1998 and Beck, Duvall and Scherrer 1998) also show hints of being giant convection cells.

Supergranules are thought to extend to 10-15 Mm beneath the solar surface, based on simple models of convective cells. It is difficult to verify these estimates since we cannot easily probe the relevant depths of the photosphere. Duvall (1998) used time-distance helioseismology to measure 3-dimensional flows associated with supergranules and found a depth of 8 Mm. However this result has not been confirmed and other results imply a far greater depth. Measurements of supergranulation rotation (eg. Snodgrass and Ulrich 1990, Beck and Schou 2000) show consistently that supergranules rotate significantly faster than the photospheric plasma and most sunspots. A comparison with rotation measurements from inversions show that supergranule rotation is consistent with a 'rooting' depth of 50 Mm (Beck 2000).

The widely accepted size scale of supergranules is approximately 30,000 km in diameter. However, recent measurements differ by a factor of almost four. Hathaway et al. (1996) studied surface flows by projecting the Doppler velocity into spherical harmonics and observed a peak in the power corresponding to 50 000 km; Hathaway et al (2000) and Duvall and Gizon (2000) found a supergranule size scale of 36,700 km. Hagenaar, Shriver, and Title (1997) found sizes of $13,000 - 18,000$ km. There is some disagreement over the effects of various techniques and which results are most representative of the supergranules.

Supergranulation lifetime studies have been hampered by the difficulty of extending observations beyond a typical observing day. Prior to the GONG project and the launch of SOHO most supergranule studies had been limited to observations from a single site with a sequence length shorter than the supergranule lifetime. Such observations can only yield estimates of the lifetime which are typically between 24 and 50 hours. (eg. Smithson 1973; Worden and Simon 1976; Duvall

1980, Wang and Zirin 1989). The work by Rogers (1970) and by Janssens (1970) used a 63 hour sequence of H_α images collected from an arctic station. However, the magnetic structures associated with the supergranulation may also have a longer lifetime (Livingston & Orrall 1974; Singh et al. 1994), and there may be a correlation between supergranule size scale and lifetime (Srikanth, Raju, Singh, 1999). Since non-convective forces could affect the magnetic network, these results must be verified with direct supergranule observations.

Duvall and Gizon (2000) have employed time-distance helioseismology of the f mode to study supergranules. They applied this technique to six days of data to determine the North-South and East-West components of the horizontal flow and have found that the Coriolis force causes divergent and convergent horizontal flows to be associated with vorticity of different signs. They further calculated the turbulent viscosity to be ~ 250 km^2/s.

2. Description of Data and Reduction Techniques

We used full-disk Doppler images from the Michelson Doppler Imager (MDI) instrument on the Solar and Heliospheric Observatory (SOHO). These data were designed for p-mode studies however, with proper filtering, they are very well suited for supergranule and steady flow studies. The data were 1024 by 1024 pixel images taken at a one-minute cadence during an eight-day period from 1996 May 24 to 1996 May 30; this period was near a minimum in solar activity.

The data were averaged to 15-minute sampling using a 31-minute tapered Gaussian weighting function adapted by Hathaway (1988) from Libbrecht and Zirin (1986). This filter decreased the signal in the frequency band 2-4 mHz by a factor of 500, effectively removing p modes and other sources of high-frequency noise. However, the length of the filter presented another problem: at disk center a feature would rotate through 2.5 pixels in 31 minutes, causing 'rotational blurring'. The images were 'derotated' to reduce this blurring by sampling each image at positions which were translated using the spectroscopic rotation profile obtained by Snodgrass and Ulrich (1990).

The MDI Doppler measurements suffered from a spurious blue shift signal which was manifest as a change of a few $\mathrm{m\,s^{-1}}$ per day. This instrumental effect was subtracted out of the averaged images along with the line-of-sight component of rotation, the limb-shift and other steady velocity fields. A sample image which shows the high quality MDI dopplergrams is shown in figure 1.

A region was extracted from each of the 768 averaged images which was continuously visible for all 8 days. The region spanned 40 degrees of longitude and 80 degrees of latitude and was centered on the equator and Carrington longitude, 60°, which crossed the disk meridian midway through the period of study. This extracted region was saved in rectangular projection sampled at 0.114285 degrees per pixels. Two sample frames of the extracted region are shown in figure 2. This region tracked the rotating sun using a solid-body rotation at the equatorial rate. Consequently, the features away from the equator appeared to drift in the retrograde direction.

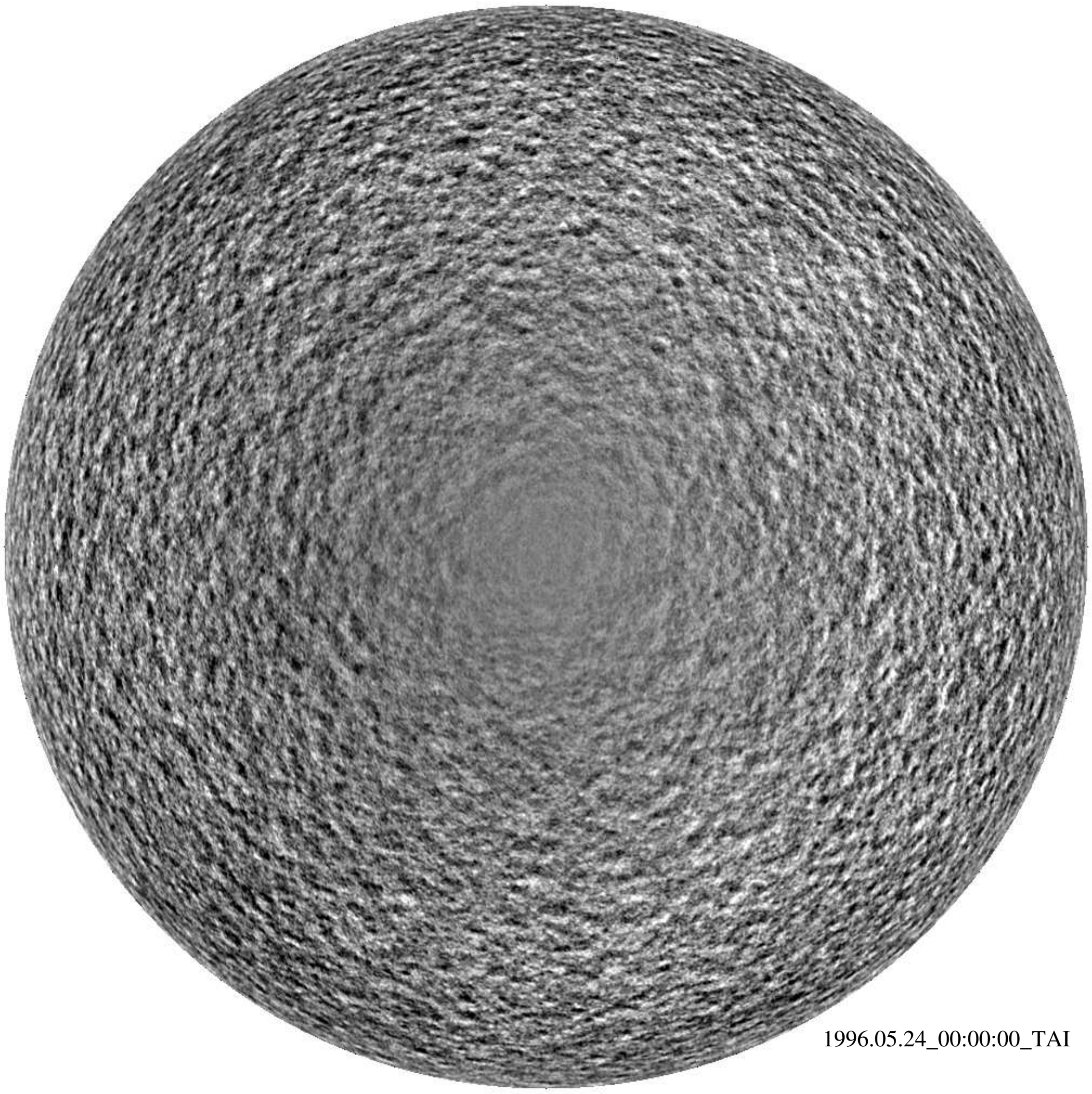

Fig. 1.— A temporally-averaged, de-rotated and detrended dopplergram from MDI. This image was produced using a tapered-Gaussian weighted average of MDI dopplergram from 31-minute sequence of images centered on 00:00:00 1996 May 24. Each image was resampled to remove motion of features due to rotation in order to decrease rotational blurring. After averaging, the large-scale, steady velocities fields were subtracted.

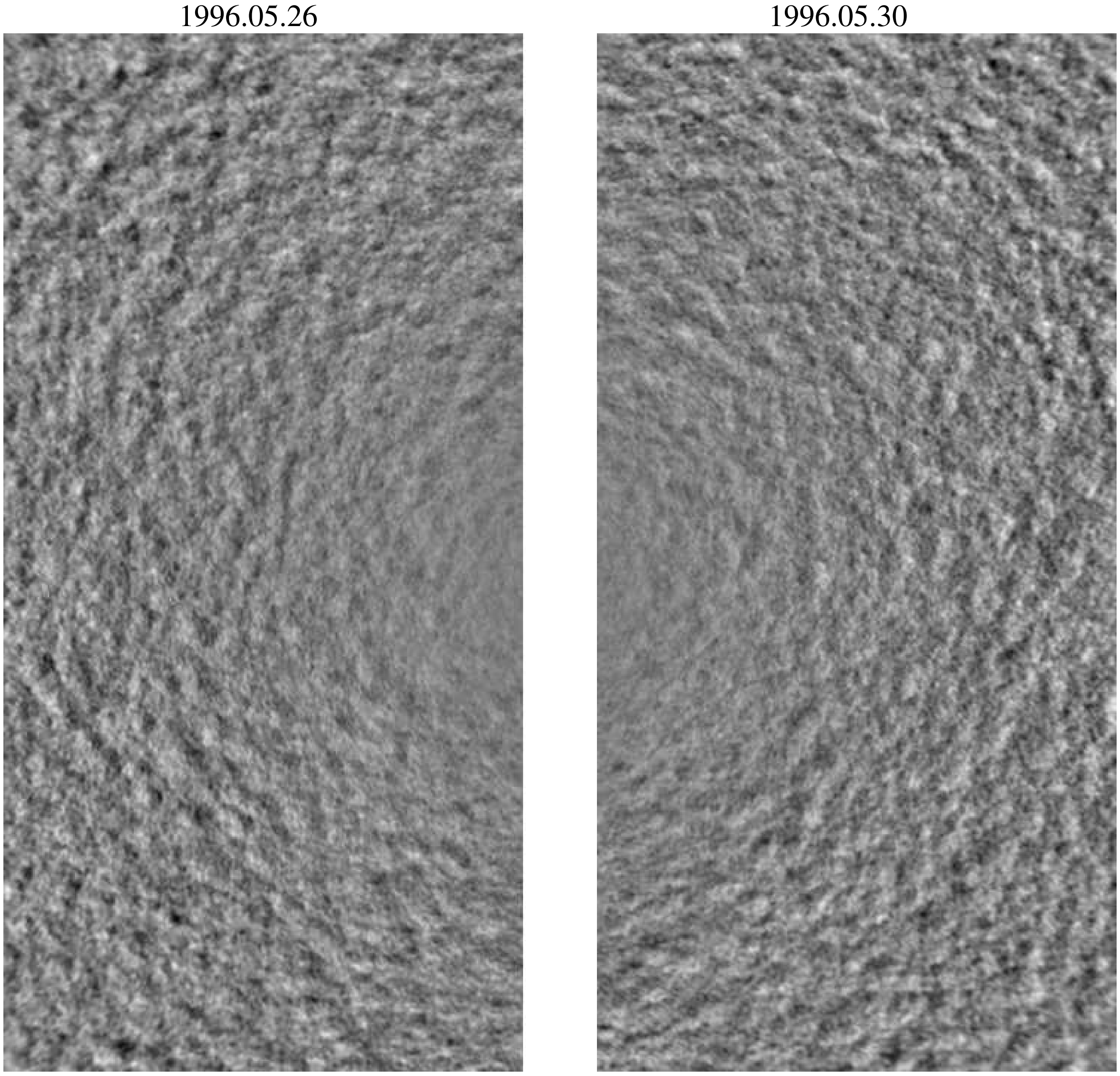

Fig. 2.— Tracked regions extracted from averaged dopplergrams. These images show the same region on the sun (latitude ±40°; Carrington longitude 40° − 80°) observed at 00:00:00 on 1996 May 26 and on 1996 May 30. Note that position of the center of disk is apparent due to the projection of supergranular velocities: the white (receding) side of the supergranules are towards the limb, the black (approaching) side are towards disk center. The disk center is just off of each frame. This projection effect is used to separate the components of the supergranule velocity.

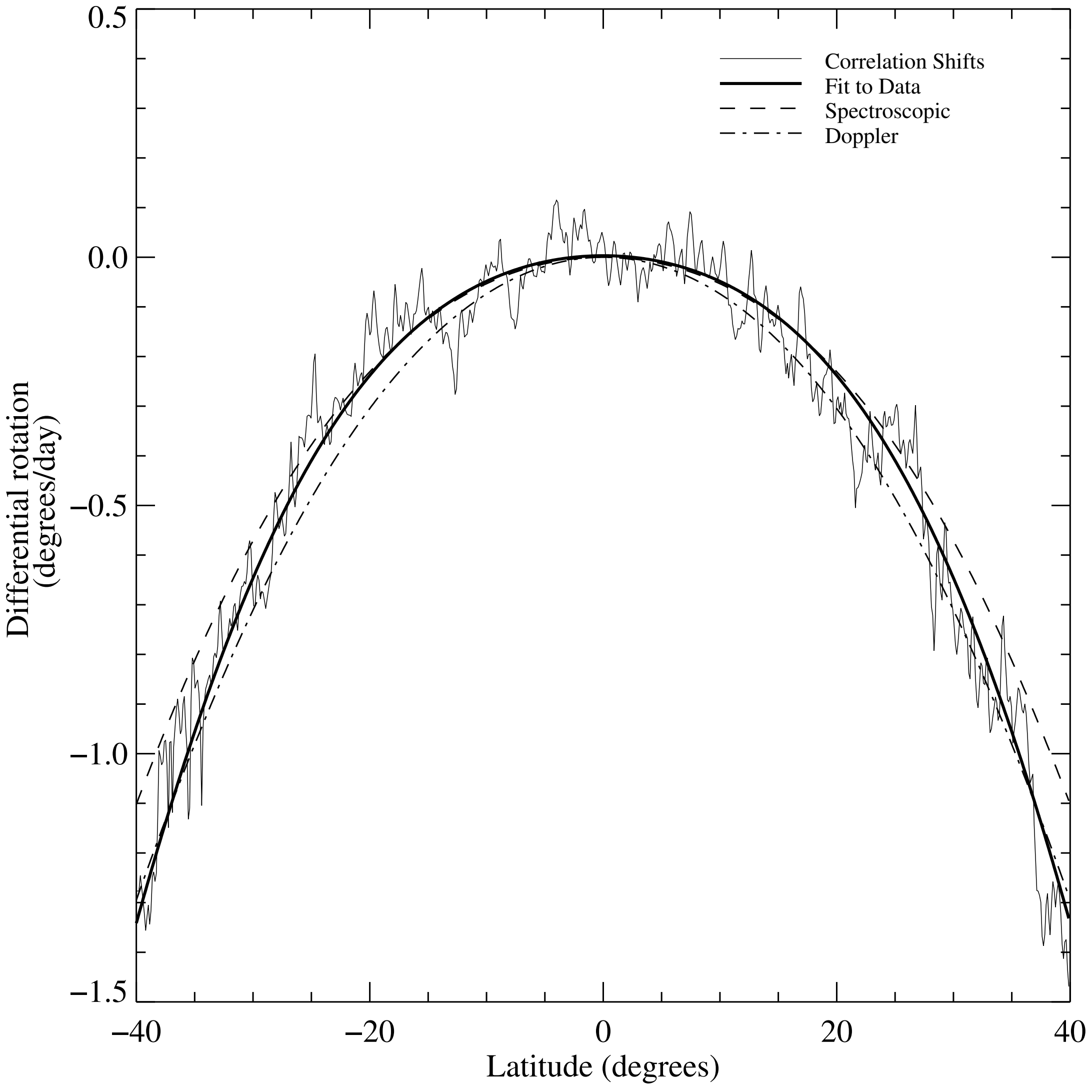

Fig. 3.— Differential rotation curves. The differential rotation curve obtained by cross-correlation of Doppler features between the tracked regions at different times is shown with a fit to the observed curve. For purposes of comparison the differential component of two rotation measurements from Snodgrass and Ulrich are shown. Note that the absolute rotation rate of supergranules is greater than the spectroscopic rate, however this plot shows the differential rotation with the equatorial rate subtracted.

The frames were assembled into a data cube with the dimensions of heliographic latitude and longitude, and time. Stacking the data into a cube allowed image planes to be extracted orthogonal to each axis for independent analysis. One such analysis determined a correction for the differential supergranulation rotation rate, which was applied to each extracted frame. The differential rate was calculated by cross-correlating rows at constant latitude between frames at different times to find the mean drift for each latitude, B. These shifts were essentially differential rotation measurements and were then fitted to a differential rotation function of the form:

$$\Omega(B) = a + b\sin^2 B + c\sin^4 B \tag{1}$$

Figure 3 shows the mean rotational shifts as a function of latitude, plotted with two differential rotation measurements from Snodgrass and Ulrich (1990). The differential rotation fit was used to align the frames over the period of tracking. A consequence of aligning the frames in this manner is that at higher latitudes some of the data was lost. At $\pm 40°$ latitude, the region for which there are 8 full days of data is $9.6°$ narrower than that at the equator; consequently, the calculations at extreme longitudes and latitudes is less significant than he calculations near the center of the tracked region. Nevertheless, there is at least 4 days of usable data for every element in the frames.

3. Analysis and Results

The specific analyses of the data are described along with the results for clarity. The first analysis was to determine typical lifetimes of supergranules and estimate the suitability of subsequent analysis. The second analysis was to extract the horizontal components of the supergranule velocities. These velocities were then studied using various methods.

3.1. Supergranulation Lifetime and Evolution

Slices at constant latitude were extracted from the data cube described in he previous section to examine supergranule evolution over time. In the time-longitude plane, each supergranulation appears as a track of eastward flow accompanied by a westward track, giving the appearance of smoke being blown from smoke stacks. A sample plane, both raw and sine-weighted, is seen in figure 5.

The lifetime of supergranules can be easy seen in this frame. Many tracks last several days, indicating that supergranules typical have a much longer lifetime than previously suspected. These tracks provide better evidence for the lifetime of supergranules than correlation or feature tracking techniques which rely on slow variations in supergranule morphology. Almost every prominent track has a lifetime exceeding two days, which was previously thought to be the upper limit of supergranule lifetime.

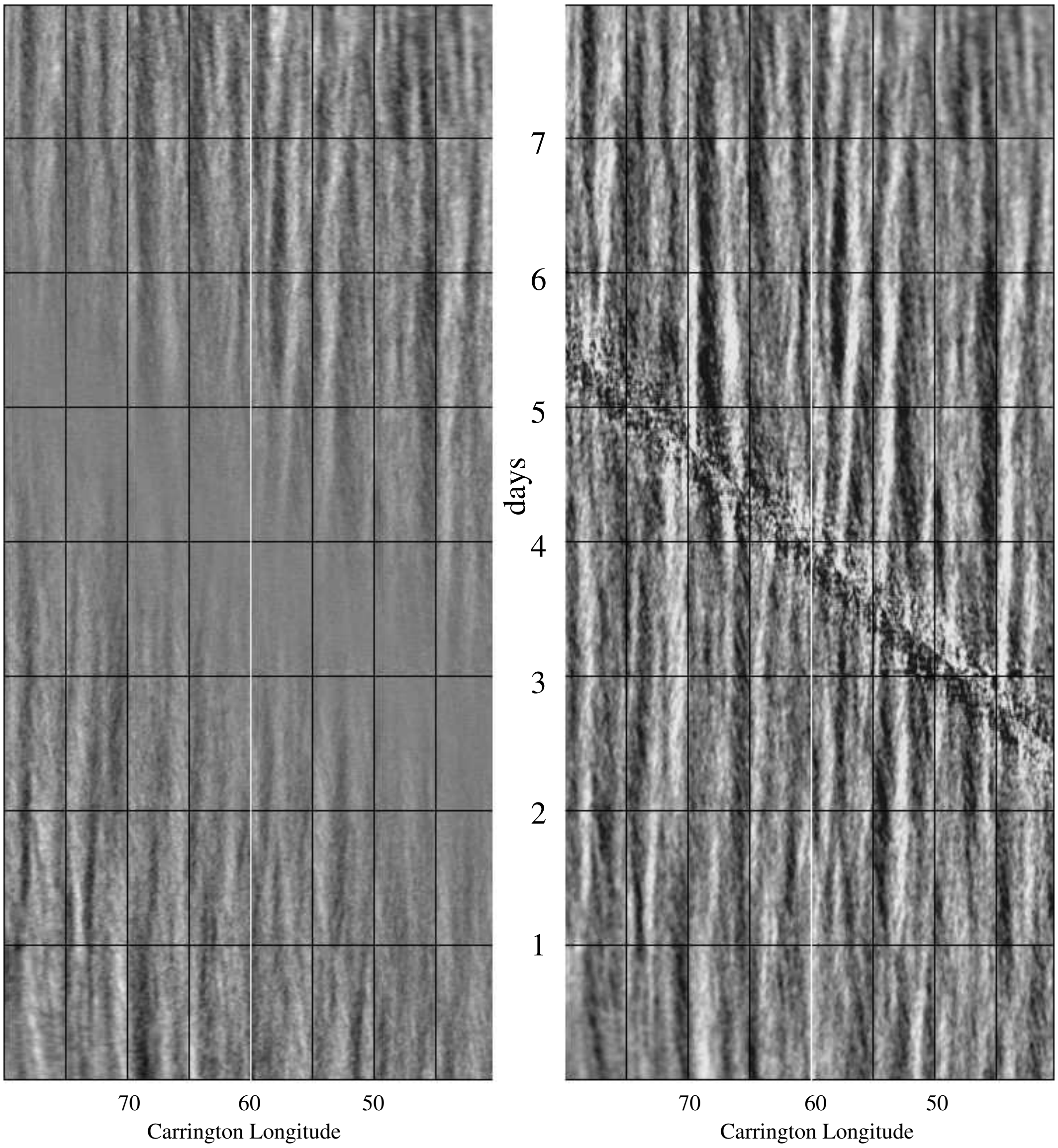

Fig. 4.— Supergranulation Evolution Track. The flow patterns of supergranules 1° south of the solar equator are displayed in these track plots. The horizontal axis is Carrington longitude and the vertical axis is time (the direction of rotation is towards the right). The left image shows Doppler velocities; the right image shows the East-West component of velocity obtained by a sine weighting, white is prograde rotation (+500 $\mathrm{m\,s^{-1}}$) and black is retrograde rotation (-500$\mathrm{m\,s^{-1}}$). Note the diagonal feature which is visible as a low amplitude zone on the left image and as a narrow seam in the right image: this is the central meridian crossing, where the East-West velocity fit is unstable. Supergranules appear as long, vertical tracks for example at longitude=75°, days = 1 - 5; longitude=55, days = 1-4; longitude=45, days=3-7. Note supergranules are 'born' at points and expand to full size and tend to fade out, rather than contract back to a point.

These supergranule tracks also provide a good means of studying supergranulation evolution. Each track begins at a point and expands over several hours to full width, continues for days and then typically fades. However, the track at longitude=45° seems to break up around day 7. Some of the tracks narrow towards the end, seemingly squeezed by younger supergranules. In these cases, the points of origin of supergranules appear to lie in the lanes between previous supergranules. It appears that supergranules 'birth' occurs at a point; however, supergranule 'death' can occur by fading, breaking up, or by collapsing back to a point.

The frame also shows supergranule motion. Some supergranule tracks change longitude over time. This cannot be explained by the tracking rate since some tracks angle towards decreasing longitude and other angle towards increasing longitude.

3.2. Supergranule Velocity Components

After applying a Gaussian filter to the images, the remaining velocities are predominantly horizontal. This can be seen in figure 1: the appearance of supergranules depends on the position on the visible disk. The rms of the line-of-sight component of the supergranule velocity varies from 242 $\mathrm{m\,s^{-1}}$ near the limb to 25.5 $\mathrm{m\,s^{-1}}$ at disk center. Due to changing the projection effect, rotation across the disk produces a time variation even when the flow is stationary. Often this interferes with steady flow studies, however, Ulrich (19XX) found that it can work to our advantage. The horizontal velocity is composed of two components, V_{EW} and V_{NS}, which contribute to the line-of-sight velocity according to:

$$V_{\mathrm{los}} = V_{\mathrm{EW}} \cos B \cos B_0 \sin(L - L_0) + V_{\mathrm{NS}} \sin(B - B_0) \cos(L - L_0) \tag{2}$$

where B and L are the solar latitude and longitude of the point in question and B_0 and L_0 are the latitude and longitude at disk center. The line-of-sight velocity, V_{los}, is the Doppler velocity, after subtracting steady flows (eg. rotation, limb redshift and meridional circulation). Since the translating of features across the visible disk is primarily due to rotation, the latitude terms are assumed constant. Therefore, the EW and NS components of the velocity can be extracted from the V_{los} by fitting to $\sin(L - L_0)$ and $\cos(L - L_0)$ terms over a large range of L. Several days of V_{los} are needed to provide a sufficient range in L to separate the V_{EW} and V_{NS} components.

Samples of the V_{los} signal are shown in figure 5. Since this feature was near the equator the V_{NS} component was negligible and is not shown. This feature was selected because it was also visible in figure 4. The irregular curves show the observed velocity signal. The smooth curves indicates the fit of $\sin(L - L_0)$ to the observed signal. Over this range of longitudes, the fit appears nearly linear. The feature crossed the central meridian just before the middle of day 4. Optimally, the amplitude of the fit is the mean East-West velocity of the supergranule over the observing period. However, since the observing period may exceed the lifetime of the supergranule the amplitude of the fit may

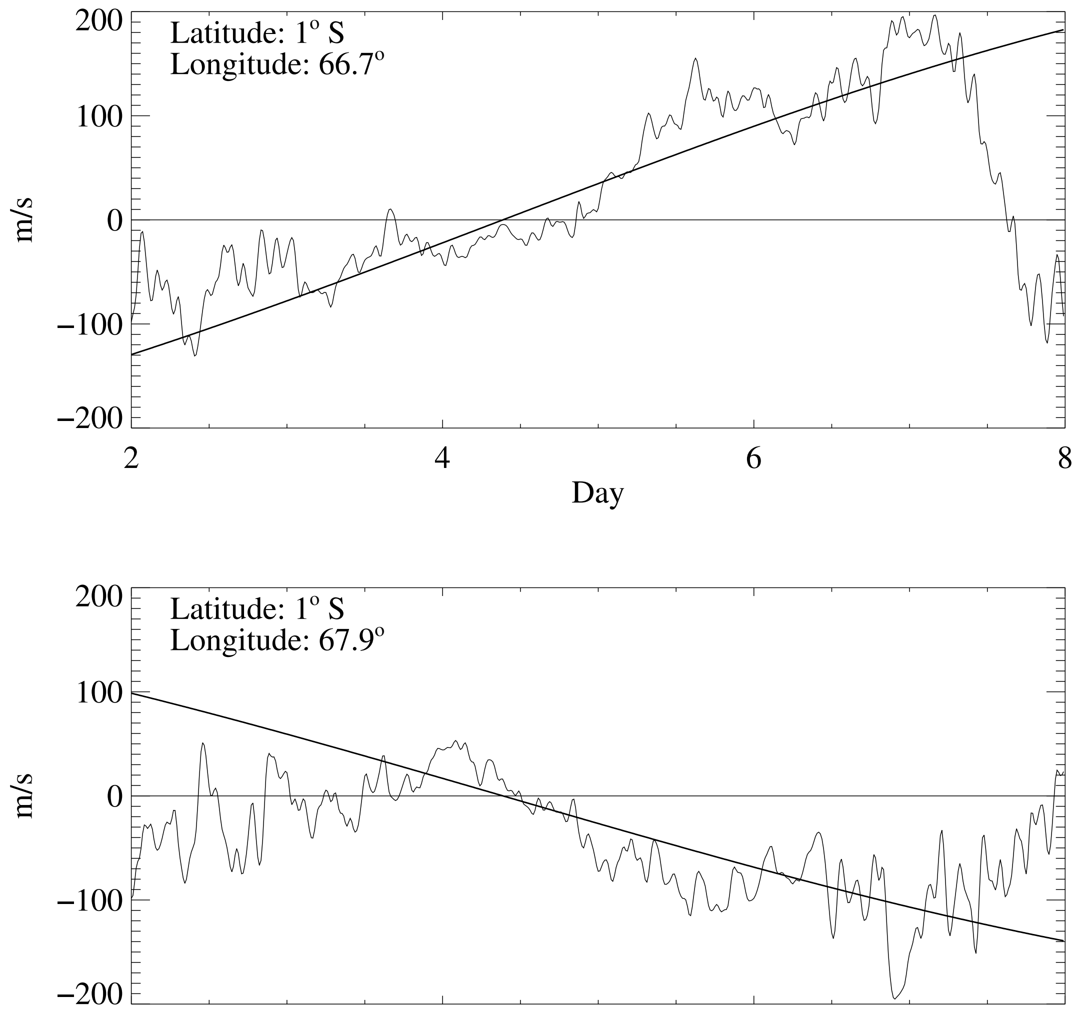

Fig. 5.— Supergranulation Velocity Signals. The velocity signals from the East and the West edge of a supergranule are shown in these plots. The heavy line is a plot of $A\sin(L - L_0)$, where A is the amplitude of the supergranule velocity.

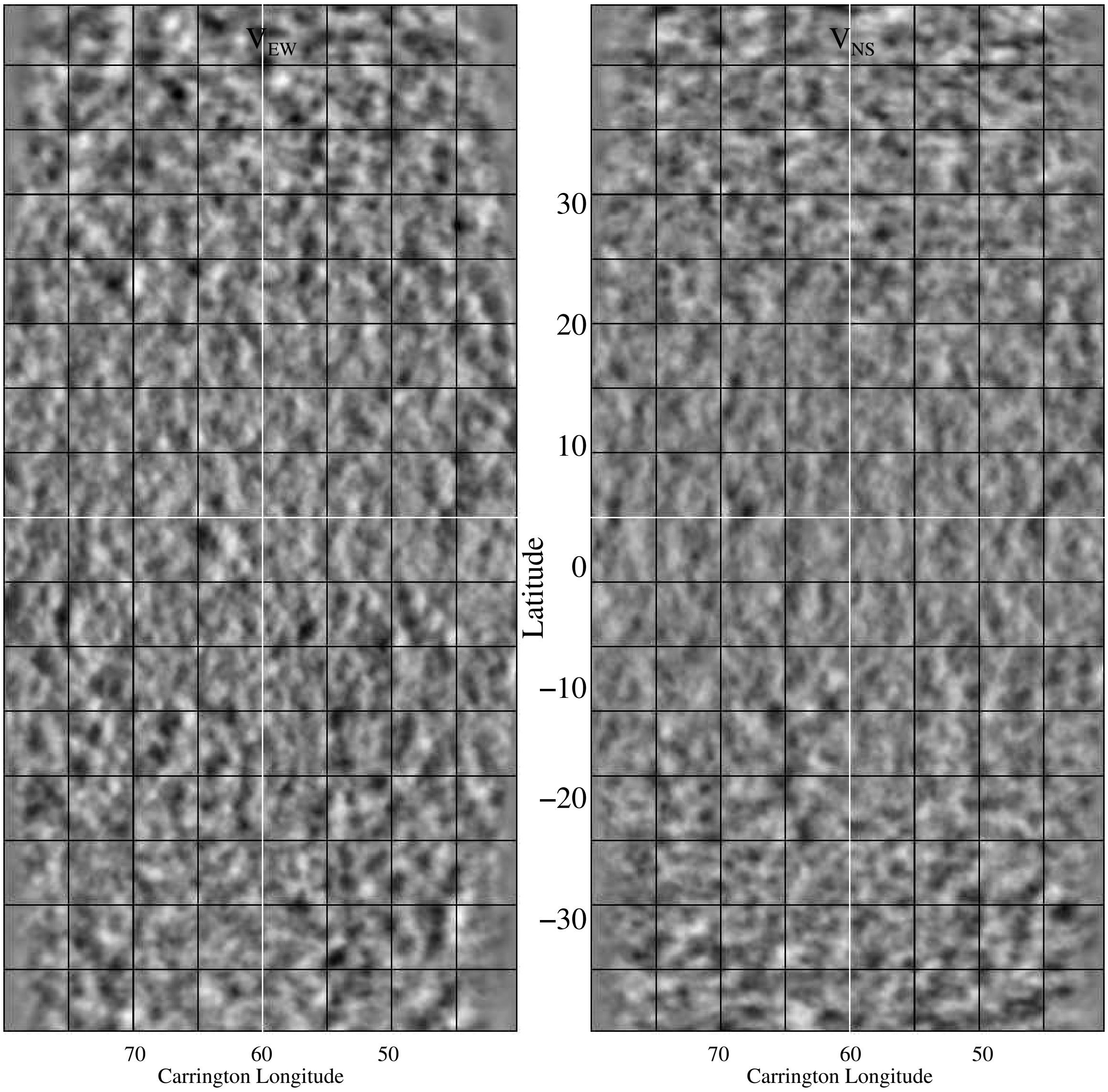

Fig. 6.— Supergranulation Velocities. The East-West and North-South components of supergranule velocities are shown here. The velocity range (black-white) is -300 $\mathrm{m\,s^{-1}}$ to 300 $\mathrm{m\,s^{-1}}$.

be less than the actual supergranule velocity. For this reason these values are considered to be upper limits of supergranule velocities.

Repeating this process for every pixel on the extracted frames produces the maps shown in figure 6. The map on the left shows the $V_{\rm EW}$ component and the map on the right shows $V_{\rm NS}$ component of the supergranule velocity after correcting for the latitude effects on the line-of-sight velocity.

The smoothly varying character and similarity of these maps indicate that the results are not noticeably affected by random noise due to errors of measurement of the velocities. This is partly due to the very large quantity of data used and partly due to the high quality of the data from the MDI instrument. We anticipated there might be some error magnification for the lowest latitude study square due to the small value of $\sin(B)$; however, there is no evident random field variation even near the equator for the $V_{\rm NS}$ component, although the features there are less distinct than they are in the $V_{\rm ew}$ map. The largest amplitudes seen in either map are relatively isolated and the typical velocity of 150 m s^{-1} is less than the nominal value for supergranulation, however, the temporal averaging technique is expected to reduce the velocity.

3.3. Supergranule Size and Cell Geometry

The maps of the $V_{\rm EW}$ and the $V_{\rm NS}$ component of supergranulation velocity provide a means to measure the size scale of supergranules. However, since the maps are rectangular grids of longitude and latitude, the longitudinal size scale of supergranules varies with latitude, so a simple 2-dimensional power spectrum is not suitable. We applied an 1-dimensional power spectra to images which were resampled to be linear in distance along the surface. The result are seen in figure 7. The supergranule size obtained by fitting to maximum of the peak is $47.6 \pm 1.5 \times 10^3$km; the centroid of the peak corresponds to $36.1 \pm 1.1 \times 10^3$ km. It must be noted that since there was some individual motion of supergranules, there was likely to be some blurring which would increase the size of the individual cells. Therefore these results must be considered upper limits to supergranulation cell size.

The geometry of supergranule cells can be best studied by combining the $V_{\rm EW}$ and $V_{\rm NS}$ components into a vector plot. Due to the large number of pixels, only a sub-raster is shown in figure 8. A classical supergranule cell can be seen centered at $B = -15.5$, $L = 70.5$ (at the bottom left of the vector plot), with a simple outflow from a single center towards the border. There is also a point of strong convergence (at $B = -17$, $L = 65$) which seems to draw from scattered sources. Many of the cells seen in this plot show significant vorticity. For example at $B = -15$, $L = 64.5$ and at $B = -19$, $L = 67$ cyclonic features are clearly visible. Duvall and Gizon (2000) have found that the vorticity of supergranules appears to be influenced by Coriolis forces using 6 days of data; however, our results show supergranules with vorticity of both signs using eight days of observation.

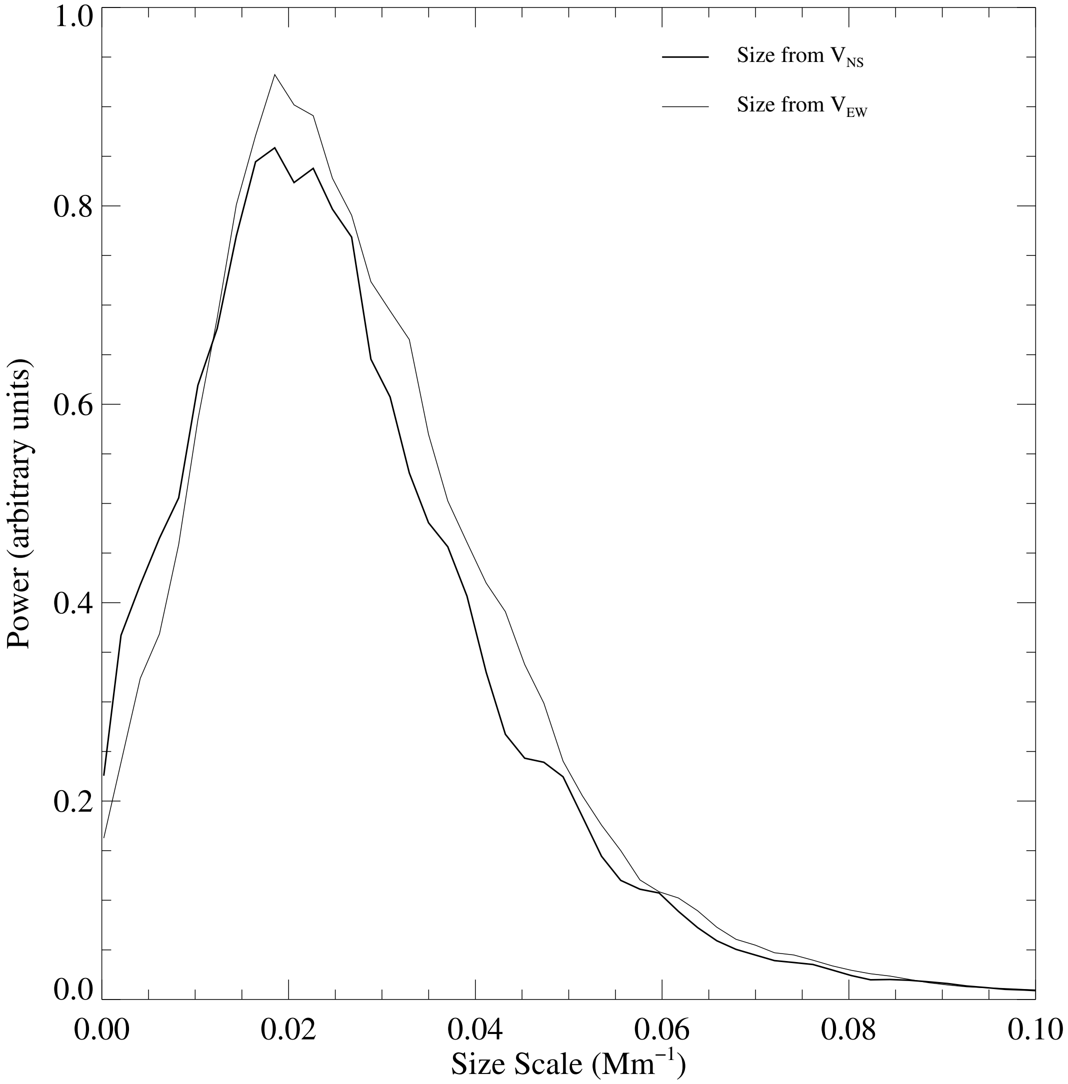

Fig. 7.— Power Spectra of Supergranulation Velocities. The size scale obtained from the East-West and North-South components of supergranule velocities are shown here

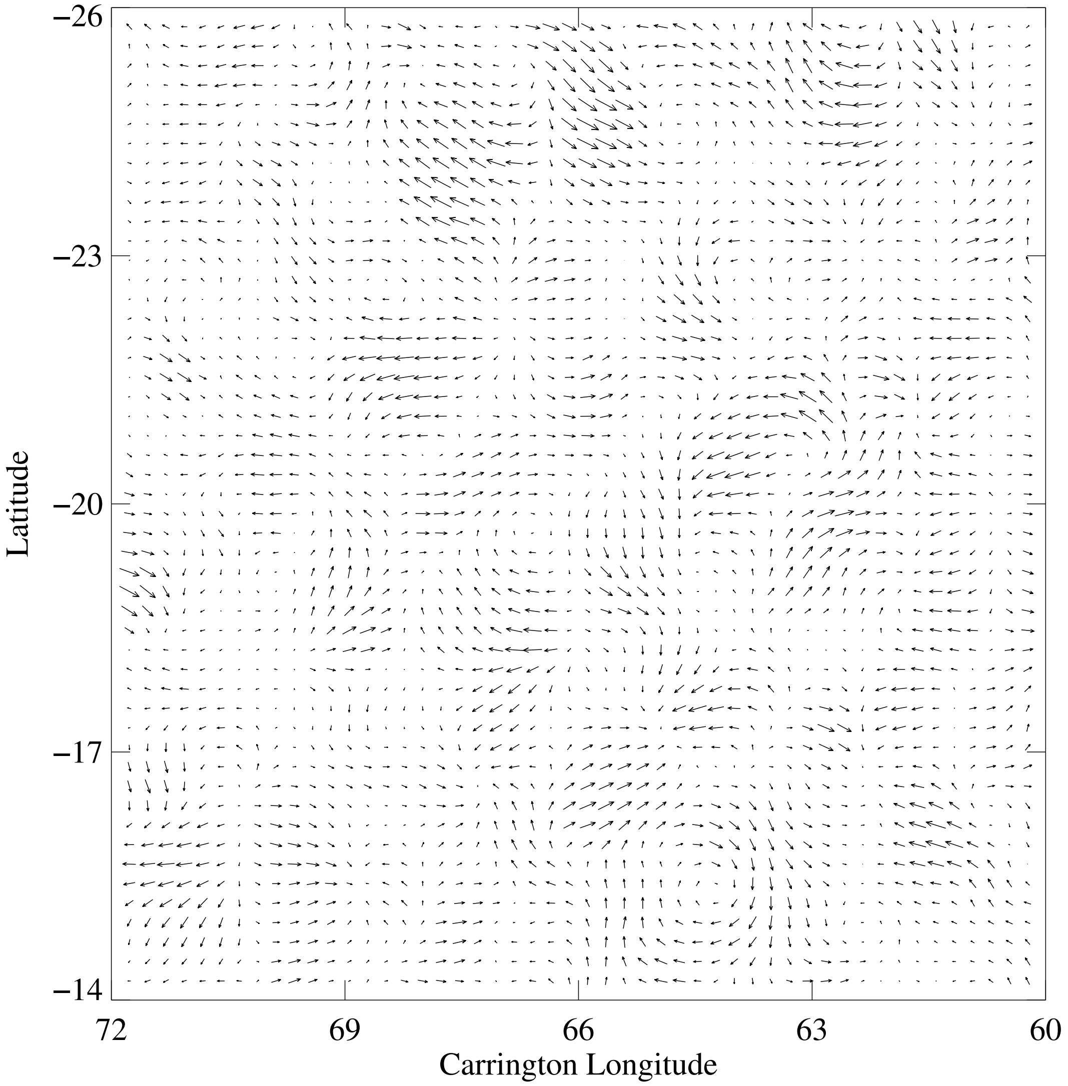

Fig. 8.— Vector Map of Supergranulation Velocities.

3.4. Angular Momentum Transport

Since supergranules appear to be influenced by the effects of rotation, it is reasonable to look for large scale rotation effects. Ward (1965) used sunspot groups as tracers and found that groups rotating faster than average typically had an equatorward trend, whereas groups rotating slower than average had a poleward trend. Ward concluded that there were eddies which transported angular momentum from the poles to the equator and could be responsible for sustaining the solar differential rotation. This work was confirmed by Coffey and Gilman (1969); Belvedere et al (1976); and Gilman and Howard (1984). The last noted that sunspots are imperfect tracers of angular momentum transport, and suggested using other methods.

Our supergranule velocities provide another means to check the results from sunspots. By multiplying the two frames from figure 6, and summing along lines of constant latitude, omitting values from regions with significant magnetic fields, we can calculate the Ward profile obtained from supergranules. The values for the southern and northern hemispheres are averaged and shown in figure 9. The SDOM is used as the uncertainty for this plot.

There is an overall trend of higher values towards higher latitudes, going to zero towards the equator. A polynomial fit to the data is shown, it lies very close to the results of Gilman and Howard (1984). This indicates that supergranulation may be connected to the process which carries angular momentum equatorward.

4. Conclusions

It is clear that some supergranules have lifetimes far in excess of previous estimates; most supergranules persist longer than two days. Previous lifetime measurements were hampered by short observing runs and underestimated supergranule lifetimes. Calculations which used supergranule lifetimes to determine properties of the convection zone should be re-evaluated.

Further, a technique suitable for studying supergranule evolution has been developed. It provides a means to gain insight to stages of development for supergranules and may help determine processes affecting supergranules as well as the magnetic network.

Supergranules display evidence of angular momentum transport, consistent with the results of Ward (1965) and Gilman and Howard (1984). This supports the models of differential rotation which carry angular momentum to the equator with eddies, it is possible that the momentum carrying eddies are on a similar size scale as supergranules and therefore interact to produce this result.

Future work, will be done to explore the angular momentum transport of eddies, using large data sets.

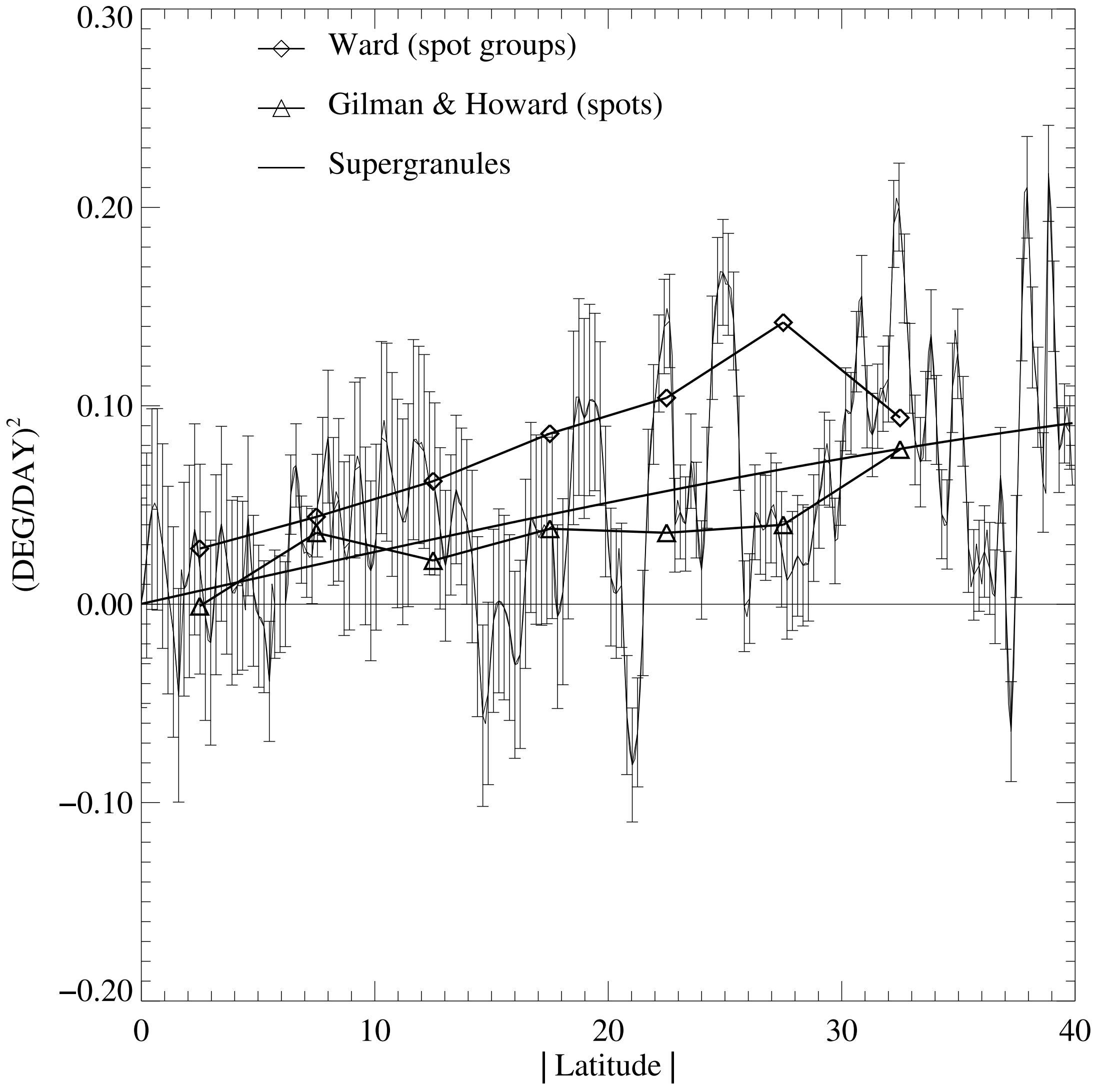

Fig. 9.— The correlation of residual longitudinal and latitudinal velocities. A positive value on this plot indicates a correlation between either a prograde and equatorward motion or a retrograde and poleward motion on the rotation sun. Thus positive values are consistent with the equator rotating faster than the poles. The line with diamonds indicates the results from Ward's measurements using sunspots as tracers. Note the slight dip to negative values is likely due to uncertainty due to the statistics of small numbers.

5. Acknowledgments

SOHO is a project of international cooperation between ESA and NASA. This research was supported by the SOI-MDI NASA grant NAS5-3077 at Stanford University and the National Solar Observatory, a division of the National Optical Astronomy Observatories which is operated by the Association of Universities for Research in Astronomy, Inc, under a cooperative agreement with the National Science Foundation.

REFERENCES

Beck, J. G. 1997, PhD Thesis, UCLA

Beck, J. G., Duvall, T. L, Jr., Scherrer, P. I. 1998, Nature, 394, 653.

Domingo, V., Fleck, B. & Poland, A. I. 1995,Sol. Phys., 162, 1

Duvall, T. L., Jr. 1980, Sol. Phys., 66, 213

Duvall Jr., T. L., Kosovichev, A. G., Scherrer, P. H., Bogart, R. S., Bush, R. I., De Forest, C., Hoeksema, J. T., Schou, J., Saba, J. L. R., Tarbell, T. D., Title, A. M., Wolfson, C. J. & Milford, P. N. 1997, Sol. Phys., 170, 63

Duvall, T.L., Jr.: 1998, in S. Korzennik and A. Wilson (eds.) *Structure and Dynamics of the Interior of the Sun and Sun-like Stars*, **SP-418**, 581.

Hart, A. B. 1954, MNRAS, 116, 38

Hart, A. B. 1956, MNRAS, 114, 17

Hathaway, D. H. 1988, Sol. Phys., 117, 1

Hathaway, D. H., Gilman, P. A., Harvey, J. W., Hill, F., Howard, R. F., Jones, H. P., Kasher, J. C., Leibacher, J. W., Pintar, J. A., & Simon, G. W. 1996, Science, 272, 1306

Hathaway, D. H., Beck, J. G., Bogart, R. S., Bachmann, K. T., Khatri, G., Petitto, J. M., Han, S., Raymond, J. Sol. Phys.*submitted.*

Howard, R. H. & Harvey, J. 1980,Sol. Phys., 12, 23-51

Kuhn, J. R., Bush, R., Bogart, R., Sa, L., Scheick, X. & Scherrer, P. 1996, Report at the December 1996 AGU Meeting in San Francisco

Leighton, R. B., Noyes, R. W. & Simon, G. W. 1962, ApJ, 135, 474

Livingston, W. C. & Orrall, F. Q. 1974, Sol. Phys., 39, 301

Scherrer, P. H., Bogart, R. S., Bush, R. I., Hoeksema, J. T., Kosovichev, A. G., Schou, J., Rosenberg, W., Springer, L., Tarbell, T. D., Title, A., Wolfson, C. J., Zayer, I. & the MDI Engineering Team 1995, Sol. Phys.162, 129

Simon, G. W., Leighton, R. B., 1964, ApJ, 140, 1120

Singh, J., Nagabhushana, B. S., Babu, G. S. D. & Uddin, W. 1994, Sol. Phys., 153, 157

Smithson, R. C. 1973, Sol. Phys., 29, 365

Srikanth, R., Raju, P., Singh, J. 1999, Sol. Phys., 184, 267

Toomre, J., Hart, J. E. & Glatzmaier, G. A. 1987, B. R. Durney & S. Sofia, The Internal Solar Angular Velocity, Reidel Dordrecht, 27

Ulrich, R. K., Boyden, J. E., Webster, L., Snodgrass, H. B., Padilla, S. P., Gilman, P. & Shieber, T. 1988, Sol. Phys., 117, 291

Ulrich, R. K. 1998, in IAU Symp. 185, New Eyes to See Inside the Sun and Stars, ed. F.-L. Deubner, J. Christensen-Dalsgaard, and D. W. Kurtz, (Dordrecht: Kluwer), 57.

Wang, H., Zirin, H. 1989, Sol. Phys., 120, 1

Ward, F., 1965, ApJ, 141, 534

Worden, S. P. & Simon, G. W. 1976, Sol. Phys., 46, 73

This preprint was prepared with the AAS LaTeX macros v5.0.